Spin Hall effect on the kagome lattice with Rashba spin-orbit interaction

Guocai Liu,[1] Ping Zhang,[2,3,*] Zhigang Wang,[2] and Shu-Shen Li[1]
[1]*Institute of Semiconductors, Chinese Academy of Sciences, Beijing 100083, People's Republic of China*
[2]*LCP, Institute of Applied Physics and Computational Mathematics, P.O. Box 8009, Beijing 100088, People's Republic of China*
[3]*Center for Applied Physics and Technology, Peking University, Beijing 100871, People's Republic of China*
(Received 7 August 2008; revised manuscript received 21 November 2008; published 22 January 2009)

We study the spin Hall effect in the kagome lattice with Rashba spin-orbit coupling. The conserved spin Hall conductance σ_{xy}^{s} (see text) and its two components, i.e., the conventional term σ_{xy}^{s0} and the spin-torque-dipole term $\sigma_{xy}^{s\tau}$, are numerically calculated, which show a series of plateaus as a function of the electron Fermi energy ϵ_F. A consistent two-band analysis, as well as a Berry-phase interpretation, is also given. We show that these plateaus are a consequence of various Fermi-surface topologies when tuning ϵ_F. In particular, we predict that compared to the case with the Fermi surface encircling the $\mathbf{\Gamma}$ point in the Brillouin zone, the amplitude of the spin Hall conductance with the Fermi surface encircling the **K** points is twice enhanced, which makes it highly meaningful in the future to systematically carry out studies of the **K**-valley spintronics.

DOI: 10.1103/PhysRevB.79.035323 PACS number(s): 73.23.−b, 71.10.Fd, 71.70.Ej

Spintronics, which combines the basic quantum mechanics of coherent spin dynamics and technological applications in information processing and storage devices, has become a very active and promising field.[1–3] The key is how to control and manipulate the spin degrees of freedom. One of the tools is using the spin-orbit (SO) couplings, which describe the interactions between the electron's orbital and spin degrees and provide the ability to manipulate the spin state via changing some external factors, such as an external electric field. It has been argued that the SO interaction leads to an intrinsic spin Hall effect (SHE),[4,5] in which a spin current flows perpendicular to an applied electric field. The initial theoretical[4–15] and experimental[16–19] studies of SHE were mainly focused on the *p* or *n* doped semiconductors (such as GaAs). Then, Murakami *et al.*[20] first identified a class of cubic materials that are usual insulators but nonetheless exhibit a finite spin Hall conductance (SHC). In those proposed "spin Hall insulators" (SHIs) the SHC is not quantized and depends on the system parameters. Later and even more fundamentally, it has been evolving into one important theme in condensed-matter physics that the SHC can be quantized in time-reversal invariant systems and thus can be used as an order parameter to characterize the emergence of new topological insulating states of matter.[21–35]

It is clear now that besides the external SO coupling (e.g., the Rashba SO coupling), the lattice structure itself also has crucial impact on the SHE through the related band structure. Different lattice structure may produce new features in the spin transport, which provides versatile choices of materials to study spin Hall transport. Motivated by this observation, in this paper we study the intrinsic SHE of the noninteracting electrons in a two-dimensional (2D) kagome lattice with Rashba SO coupling. Since our attention is solely on the SHE character brought about by the interplay between the kagome lattice structure and the Rashba SO coupling, thus unlike most of previous works, the kagome lattice considered in this paper is nonmagnetic. The nonmagnetic kagome lattice structure has been either fabricated by modern patterning techniques[36,37] or observed in reconstructed semiconductor surfaces.[38] In the former case, remarkably, the electron filling factor (namely, the Fermi energy) can be readily controlled by applying a gate voltage.[39] Our lattice model is free from the constraint imposed on the $\mathbf{k}\cdot\mathbf{p}$ approximation used in the extensively studied GaAs two-dimensional electron gas (2DEG), in which the $\mathbf{k}\cdot\mathbf{p}$ Hamiltonian is only valid around the Γ point in the Brillouin zone (BZ). In contrast, our lattice model allows for any electron filling, which results in various Fermi-surface topologies, which in turn, as will be shown below, produces profound effects on the spin Hall transport.

To calculate the SHC and build a correspondence between spin current and spin accumulation in the present SO-coupled system, in which the electron spin (s_z here to be specific) is not conserved, we use a "conserved" spin current $\mathcal{J}_s$,[40] which is a sum of the conventional spin current $\mathbf{J}_s \equiv \frac{1}{2}\{\mathbf{v}, s_z\}$ and a spin torque dipole $\mathbf{P}_\tau \equiv \mathbf{r}\dot{s}_z$. This spin current satisfies both the spin continuity equation $\partial_t s_z + \nabla\cdot\mathcal{J}_s = 0$ (within spin-relaxation time) and Onsager relation.[41] If the spin itself is conserved (as in quantum SHIs), $\mathcal{J}_s$ is reduced to $\mathbf{J}_s$. In general, the spin transport coefficient $\sigma_{\mu\nu}^{s}$ under new definition is composed of two parts, i.e., the conventional part $\sigma_{\mu\nu}^{s0}$ and the spin torque dipole correction $\sigma_{\mu\nu}^{s\tau}$. A general Kubo formula[40,42] for the spin transport coefficients is employed in this paper to calculate the SHC.

Let us consider the tight-binding model for independent electrons on the 2D kagome lattice (Fig. 1). The spin-independent part of the Hamiltonian is given by

$$H_0 = t_0 \sum_{\langle i,j\rangle} (c_{i\alpha}^{\dagger} c_{j\alpha} + \text{H.c.}), \tag{1}$$

where $t_{ij}=t_0$ is the hopping amplitude between the nearest-neighbor link $\langle i,j\rangle$ and $c_{i\alpha}^{\dagger}$ ($c_{i\alpha}$) is the creation (annihilation) operator of an electron with spin α (up or down) on lattice site i. For simplicity, we choose $t_0=1$ as the energy unit and the distance a between the nearest sites as the length unit throughout this paper.

Hamiltonian (1) can be diagonalized in the momentum space as

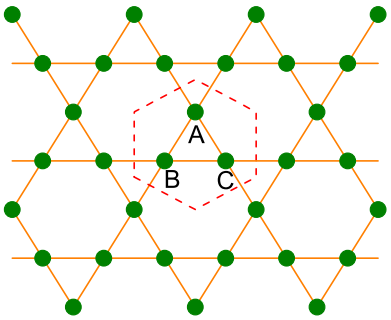

FIG. 1. (Color online) Schematic picture of the 2D kagome lattice. The dashed lines represent the Wigner-Seitz unit cell, which contains three independent sites (A, B, and C).

$$\mathcal{H}_0 = \sum_{\mathbf{k}} \psi_{\mathbf{k}}^{+}[H_0(\mathbf{k}) \otimes \mathbf{I}_{2\times 2}]\psi_{\mathbf{k}}, \tag{2}$$

where the 2×2 unit matrix $\mathbf{I}_{2\times 2}$ denotes the spin degeneracy in Hamiltonian H_0 and $\psi_{\mathbf{k}}=(c_{A\mathbf{k}\uparrow}, c_{B\mathbf{k}\uparrow}, c_{C\mathbf{k}\uparrow}, c_{A\mathbf{k}\downarrow}, c_{B\mathbf{k}\downarrow}, c_{C\mathbf{k}\downarrow})^{\mathrm{T}}$ is the six-component electron field operator, which includes the three lattice sites s $(=A,B,C)$ in the Wigner-Seitz unit cell shown in Fig. 1. Each component of $\psi_{\mathbf{k}}$ is the Fourier transform of $c_{i\alpha}$, i.e.,

$$\psi_{s\alpha}(\mathbf{k}) = \sum_{mn} c_{mns\alpha} e^{i\mathbf{k}\cdot\mathbf{r}_{mns}}, \tag{3}$$

where we have changed notation $i \to (mns)$ by using (mn) to label the kagome unit cells. $H_0(\mathbf{k})$ is a 3×3 spinless matrix given by

$$H_0(\mathbf{k}) = \begin{pmatrix} 0 & 2\cos(\mathbf{k}\cdot\mathbf{a}_1) & 2\cos(\mathbf{k}\cdot\mathbf{a}_3) \\ 2\cos(\mathbf{k}\cdot\mathbf{a}_1) & 0 & 2\cos(\mathbf{k}\cdot\mathbf{a}_2) \\ 2\cos(\mathbf{k}\cdot\mathbf{a}_3) & 2\cos(\mathbf{k}\cdot\mathbf{a}_2) & 0 \end{pmatrix}, \tag{4}$$

where $\mathbf{a}_1=(-1/2,-\sqrt{3}/2)$, $\mathbf{a}_2=(1,0)$, and $\mathbf{a}_3=(-1/2,\sqrt{3}/2)$ represent the displacements in a unit cell from the A to B site, from the B to C site, and from the C to A site, respectively. In this notation, the first BZ is a hexagon with the corners of $\mathbf{K}=\pm(2\pi/3)\mathbf{a}_1$, $\pm(2\pi/3)\mathbf{a}_2$, and $\pm(2\pi/3)\mathbf{a}_3$.

The energy spectrum for spinless Hamiltonian $H_0(\mathbf{k})$ is characterized by one dispersionless flat band $(\epsilon_{1\mathbf{k}}^{(0)}=-2)$, which reflects the fact that the 2D kagome lattice is a line graph of the honeycomb structure[43] and two dispersive bands, $\epsilon_{2(3)\mathbf{k}}^{(0)}=1\mp\sqrt{4b_{\mathbf{k}}-3}$, with $b_{\mathbf{k}}=\Sigma_{i=1}^{3}\cos^2(\mathbf{k}\cdot\mathbf{a}_i)$. These two dispersive bands touch at the corners ($\mathbf{K}$ points) of the BZ and exhibit Dirac-type energy spectra, $\epsilon_{2(3)\mathbf{k}}^{(0)}=(1\mp\sqrt{3}|\mathbf{k}-\mathbf{K}|)$, which implies a "particle-hole" symmetry with respect to the Fermi energy $\epsilon_F=1$. The corresponding eigenstates of $H_0(\mathbf{k})$ are given by

$$|u_{n\mathbf{k}}^{(0)}\rangle = G_{n\mathbf{k}}(q_{1\mathbf{k}}, q_{2\mathbf{k}}, q_{3\mathbf{k}})^{\mathrm{T}}, \tag{5}$$

where the expressions of the components $q_{i\mathbf{k}}$ and the normalized factor $G_n(\mathbf{k})$ for each band are given in Table I. At two equivalent BZ edge points $\mathbf{M}=(0,\pm\pi/\sqrt{3})$, one can find that the wave function $|u_{n\mathbf{k}}^{(0)}\rangle$ is ill-defined since both its denominator and numerator are zero at these two points.

TABLE I. The expressions for the coefficients in Eq. (5) with $x_i=\mathbf{k}\cdot\mathbf{a}_i$.

q_{1k}	$1/2[\epsilon_{nk}^{(0)2}-4\cos^2 x_2]$
q_{2k}	$\epsilon_{nk}^{(0)}\cos x_1+2\cos x_2\cos x_3$
q_{3k}	$\epsilon_{nk}^{(0)}\cos x_3+2\cos x_2\cos x_1$
G_{nk}^{-2}	$2b_k\epsilon_{nk}^{(0)2}+[4b_k-3\epsilon_{nk}^{(0)2}]\cos^2 x_2+6(b_k-1)\epsilon_{nk}^{(0)}$

When an external Rashba SO coupling, which can be realized by a perpendicular electric field or by interaction with a substrate, is taken into account in the 2D kagome lattice model, the spin degeneracy will be lifted. The tight-binding expression for this external Rashba term can be given as follows:

$$H_{\mathrm{SO}} = i\frac{\lambda}{\hbar}\sum_{\langle ij\rangle\alpha\beta} c_{i\alpha}^{\dagger}(\sigma\times\hat{\mathbf{d}}_{ij})_z c_{j\beta}, \tag{6}$$

where λ is the Rashba coefficient, σ are the Pauli matrices, and $\hat{\mathbf{d}}_{ij}$ is a vector along the bond the electron traverses going from site j to i. Taking the Fourier transform [Eq. (3)] and considering the $\psi_{\mathbf{k}}$ below Eq. (2), we have $H_{\mathrm{SO}}=\Sigma_{\mathbf{k}}\psi_{\mathbf{k}}^{+}H_{\mathrm{SO}}(\mathbf{k})\psi_{\mathbf{k}}$ with

$$H_{\mathrm{SO}}(\mathbf{k}) = \begin{pmatrix} 0 & H_R(\mathbf{k}) \\ H_R^{*}(\mathbf{k}) & 0 \end{pmatrix} \tag{7}$$

and

$$H_R(\mathbf{k}) = \lambda\begin{pmatrix} 0 & e^{i(\pi/6)}\sin(\mathbf{k}\cdot\mathbf{a}_1) & -e^{-i(\pi/6)}\sin(\mathbf{k}\cdot\mathbf{a}_3) \\ e^{i(\pi/6)}\sin(\mathbf{k}\cdot\mathbf{a}_1) & 0 & -i\sin(\mathbf{k}\cdot\mathbf{a}_2) \\ -e^{-i(\pi/6)}\sin(\mathbf{k}\cdot\mathbf{a}_3) & -i\sin(\mathbf{k}\cdot\mathbf{a}_2) & 0 \end{pmatrix}. \tag{8}$$

Inclusion of the Rashba SO term in the Hamiltonian makes the analytical derivation of the eigenstates $|u_{n\mathbf{k}}\rangle$ $(n=1,\ldots,6)$ and eigenenergies $\epsilon_{n\mathbf{k}}$ very tedious. At the general k points, these quantities can only be numerically obtained. At some high-symmetry k points, however, they can be approximately obtained, which turns out to provide a great help in analyzing SHC.

The energy spectrum for the total Hamiltonian $H(\mathbf{k})$

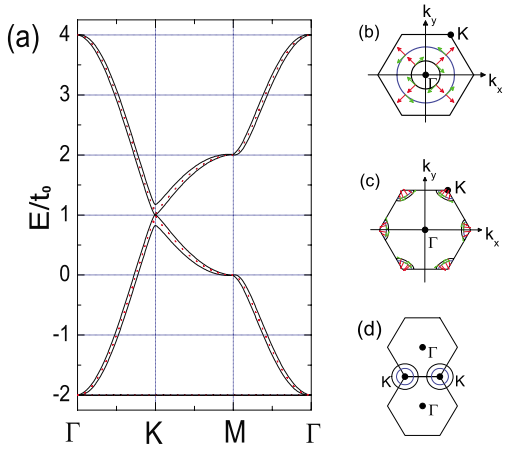

FIG. 2. (Color online) (a) Energy spectrum of the 2D kagome lattice with Rashba SO constant $\lambda=0.1$ (solid curves). (b) and (c) show the Fermi surfaces in the regimes $-2<\epsilon_F<0$ and $0<\epsilon_F<1$, respectively. Directions of the electron's velocity and spin polarization are also shown by red and green arrows, respectively. (d) Reconstructed Fermi surface around the two **K** points by gluing the six sheets of the Fermi surface in (c). For comparison, the energy spectrum in the absence of the Rashba SO coupling is also plotted; see the dashed curves in (a). One can see that the lowest flat band is immune to the Rashba SO coupling.

$=H_0(\mathbf{k})+H_{\mathrm{SO}}(\mathbf{k})$ is numerically calculated and shown in Fig. 2 (solid curves) along the high-symmetry lines ($\mathbf{\Gamma}\rightarrow\mathbf{K}$, $\mathbf{K}\rightarrow\mathbf{M}$, and $\mathbf{M}\rightarrow\mathbf{\Gamma}$) in the BZ. The Rashba coefficient is chosen to be $\lambda=0.1$. Note that in this paper, our only concern is the physically reasonable limit of $\lambda\ll t_0$ (t_0 is chosen to be unity). For comparison we also plot in Fig. 2 (dashed curves) the energy spectrum in the absence of the Rashba SO coupling ($\lambda=0$). For the middle and upper bands, one can see that the spin degeneracies are generally lifted in the BZ with the exception at **Γ** and **M** points, at which the energy is still spin degenerate due to time-reversal symmetry. The most prominent splitting occurs at the corners (**K** points) of the BZ. However, this splitting does not change the Dirac-type nature of the dispersions around these corners. Also, there still exist contacts at these corners between one middle band and one upper band, as seen from Fig. 2. For the lowest flat band, on the other hand, it reveals in Fig. 2 that the Rashba splitting is negligibly small, and there is no observable SO effect on this flat band. The two-band approximation given below will also indicate this fact.

The conserved SHC σ_{xy}^{s} includes two components, $\sigma_{xy}^{s}=\sigma_{xy}^{s0}+\sigma_{xy}^{s\tau}$, where σ_{xy}^{s0} is the conventional part and $\sigma_{xy}^{s\tau}$ comes from the spin torque dipole correction. In terms of the band energies $\epsilon_{n\mathbf{k}}$ and states $|u_{n\mathbf{k}}\rangle$ of $H(\mathbf{k})=H_0(\mathbf{k})+H_{\mathrm{SO}}(\mathbf{k})$, these two SHC components are given by[40,42]

$$\sigma_{xy}^{s0}=-e\hbar\sum_{n\neq n',\mathbf{k}}[f(\epsilon_{n\mathbf{k}})-f(\epsilon_{n'\mathbf{k}})]\times\frac{\mathrm{Im}\langle u_{n\mathbf{k}}|\frac{1}{2}\{v_x,s_z\}|u_{n'\mathbf{k}}\rangle\langle u_{n'\mathbf{k}}|v_y|u_{n\mathbf{k}}\rangle}{(\epsilon_{n\mathbf{k}}-\epsilon_{n'\mathbf{k}})^2+\eta^2} \tag{9}$$

and

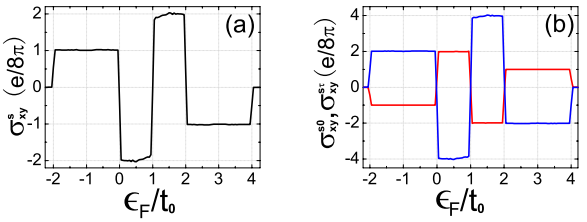

FIG. 3. (Color online) (a) The conserved SHC σ_{xy}^{s} and (b) its two components σ_{xy}^{0} (red curve) and σ_{xy}^{τ} (blue curve) as functions of the electron Fermi energy for the Rashba coefficient $\lambda=0.1$.

$$\sigma_{xy}^{s\tau}=-e\hbar\lim_{\mathbf{q}\rightarrow 0}\frac{1}{q_x}\sum_{n\neq n',\mathbf{k}}[f(\epsilon_{n\mathbf{k}})-f(\epsilon_{n'\mathbf{k}+q})]\times\frac{\mathrm{Re}\langle u_{n\mathbf{k}}|\tau(\mathbf{k},\mathbf{q})|u_{n'\mathbf{k}+\mathbf{q}}\rangle\langle u_{n'\mathbf{k}+\mathbf{q}}|v_y(\mathbf{k},\mathbf{q})|u_{n\mathbf{k}}\rangle}{(\epsilon_{n\mathbf{k}}-\epsilon_{n'\mathbf{k}+\mathbf{q}})^2+\eta^2}, \tag{10}$$

where $\tau(\mathbf{k},\mathbf{q})\equiv\frac{1}{2}[\tau(\mathbf{k})+\tau(\mathbf{k}+\mathbf{q})]$ with $\tau(\mathbf{k})=\dot{s}_z$, $\mathbf{v}(\mathbf{k},\mathbf{q})$ is given in the same manner, and $f(\epsilon_{n\mathbf{k}})$ is the equilibrium Fermi function. The limit of $\eta\rightarrow 0$ should be taken at the last step of the calculation. In the present six-band model the spin operator s_z should be written as $\mathbf{I}_{3\times 3}\otimes\sigma_z$ in unit of $\hbar/2$.

We have numerically calculated the SHC as a function of the electron Fermi energy ϵ_F. The main results for zero temperature are shown in Fig. 3, in which Fig. 3(a) plots the conserved SHC σ_{xy}^{s}, while Fig. 3(b) plots its two components, i.e., the conventional term σ_{xy}^{s0} and the spin torque dipole term $\sigma_{xy}^{s\tau}$. For comparison, the value of the Rashba SO coefficient λ used in Fig. 3 is the same as in Fig. 2 (solid curves). One can see that within the whole range of the electron filling (Fermi energy), the two components σ_{xy}^{s0} and $\sigma_{xy}^{s\tau}$ always oppose each other. In fact, this feature of opposite signs of the two components σ_{xy}^{s0} and $\sigma_{xy}^{s\tau}$ (if both of them are nonzero) is robust and does not depend on specific models.[44] Remarkably, the amplitude of $\sigma_{xy}^{s\tau}$ is twice as large as that of σ_{xy}^{s0}, which results in the consequence that the total SHC σ_{xy}^{s} has an overall sign change with respect to the conventional SHC σ_{xy}^{s0}. As will be shown below, around the **Γ** point the present model can be mapped into the simple Rashba 2DEG model. Together with the previous studies of the conserved SHC in the Rashba 2DEG,[42] one can see the key role played by the spin-torque-dipole term, which in some special cases tends to overwhelm the conventional SHC by an opposite contribution. On the other hand, considering the variation in the SHC as a function of electron Fermi energy, the present results in the 2D kagome lattice display more profound features compared to those in the 2DEG system. In fact, it reveals in Fig. 3 that the conserved SHC and its two components display four plateaus as a function ϵ_F. When the electron filling satisfies the condition $-2.0<\epsilon_F<0$, the value of σ_{xy}^{s} is $e/8\pi$ while the values of σ_{xy}^{s0} and $\sigma_{xy}^{s\tau}$ are $-e/8\pi$ and $e/4\pi$, respectively. When the electron filling increases to satisfy $0<\epsilon_F<1.0$, then the conserved SHC jumps down to $\sigma_{xy}^{s}=-e/4\pi$ while its two components also jump to $\sigma_{xy}^{s0}=e/4\pi$ and $\sigma_{xy}^{s\tau}=-e/2\pi$. When the Fermi energy continues to increase to satisfy $1.0<\epsilon_F<2.0$, then the conserved SHC

jumps up to $\sigma_{xy}^{s}=e/4\pi$, while its two components also jump to $\sigma_{xy}^{s0}=-e/4\pi$ and $\sigma_{xy}^{s\tau}=e/2\pi$. Finally, when the Fermi energy satisfies the condition $2.0<\epsilon_F<4.0$, then the conserved SHC jumps down to $\sigma_{xy}^{s}=-e/8\pi$, while its two components jump to $\sigma_{xy}^{s0}=e/8\pi$ and $\sigma_{xy}^{s\tau}=-e/4\pi$.

We turn now to understand the physics embodied in Fig. 3. Since we are dealing with the usual case of weak SO coupling ($\lambda \ll t_0$), thus the SHC behavior in Fig. 3 should be mainly due to the coupling of the two Rashba SO-split bands and can be described by an effective two-band approximation. To be more clear, let us treat the Rashba SO term as a perturbation to the spinless Hamiltonian $H_0(\mathbf{k})$. The expressions for the unperturbed eigenenergies $\epsilon_{n\mathbf{k}}^{(0)}$ $(n=1,2,3)$ and eigenstates $|u_{n\mathbf{k}}^{(0)}\rangle$ have been given above. Then, the effective two-band Hamiltonian originating from $\epsilon_{n\mathbf{k}}^{(0)}$ and $|u_{n\mathbf{k}}^{(0)}\rangle$ is obtained by taking into account the Rashba SO splitting as follows:

$$\bar{H}_n(\mathbf{k})=\epsilon_{n\mathbf{k}}^{(0)}\mathbf{I}_{2\times 2}+\begin{pmatrix}0 & \Delta_{n\mathbf{k}}e^{i\varphi_{n\mathbf{k}}}\\ \Delta_{n\mathbf{k}}e^{-i\varphi_{n\mathbf{k}}} & 0\end{pmatrix}, \tag{11}$$

where the basis set to expand $\bar{H}_n(\mathbf{k})$ consists of $|u_{n\mathbf{k}}^{(0)}\rangle\otimes|\uparrow\rangle$ and $|u_{n\mathbf{k}}^{(0)}\rangle\otimes|\downarrow\rangle$. Here the coefficients $\Delta_{n\mathbf{k}}$ and $\varphi_{n\mathbf{k}}$ are defined by

$$\begin{aligned}\Delta_{n\mathbf{k}}\cos\varphi_{n\mathbf{k}}&=-\frac{\sqrt{3}\lambda}{2}G_n^2(\mathbf{k})(\epsilon_{n\mathbf{k}}^{(0)}+2)\\&\quad\times(\epsilon_{n\mathbf{k}}^{(0)2}-4\cos^2 k_x)\cos k_x\sin(\sqrt{3}k_y),\\ \Delta_{n\mathbf{k}}\sin\varphi_{n\mathbf{k}}&=-\frac{\lambda}{2}G_n^2(\mathbf{k})(\epsilon_{n\mathbf{k}}^{(0)}+2)\sin k_x\\&\quad\times[4\epsilon_{n\mathbf{k}}^{(0)}\cos k_x+(\epsilon_{n\mathbf{k}}^{(0)2}+4\cos^2 k_x)\cos(\sqrt{3}k_y)].\end{aligned} \tag{12}$$

The eigenenergies of $\bar{H}_n(\mathbf{k})$ are

$$\epsilon_{n\mathbf{k}}^{(\pm)}=\epsilon_{n\mathbf{k}}^{(0)}\pm\Delta_{n\mathbf{k}}. \tag{13}$$

The corresponding eigenstates are given by

$$|u_{n\mathbf{k}}^{(\pm)}\rangle=\frac{1}{\sqrt{2}}(\pm e^{i\varphi_{n\mathbf{k}}},1)^{\mathrm{T}}. \tag{14}$$

As a result, the total Hamiltonian can now be approximated by

$$\bar{H}(\mathbf{k})=\oplus_{n=1}^{3}\bar{H}_n(\mathbf{k}). \tag{15}$$

This two-band approximation proves to work very well in the weak Rashba SO coupling limit. In particular, one can see that the lowest flat band ($\epsilon_{1\mathbf{k}}^{(0)}=-2$) is not split by the Rashba SO coupling in the first order in λ since the quantity $\Delta_{1\mathbf{k}}e^{i\varphi_{1\mathbf{k}}}$ is zero, and as a result, the off-diagonal element in Eq. (11) $(n=1)$ vanishes. This perturbative analysis agrees well with the exact numerical result in Fig. 2, which shows that the original flat band $\epsilon_{1\mathbf{k}}^{(0)}$ keeps nearly dispersionless upon weak Rashba SO interaction. As a result, the contribution of these two spin almost-degenerate flat bands to the SHC should be negligibly small, which has been verified by our numerical test.

Thus, the finite SHC in Fig. 3 is ascribed to the contributions from the two (SO-split) middle or the two upper bands, depending on the position of the Fermi energy. Remarkably, there is a particle-hole symmetry between the middle and upper bands with respect to their contact energy plane. As a consequence, the SHC is antisymmetric with respect to the Fermi energy $\epsilon_F=1.0$, as revealed in Fig. 3. Keeping this fact in mind, our remaining discussion of Fig. 3 will focus on the two SHC plateaus and the transition between them when scanning ϵ_F through the middle bands. According to Eqs. (9) and (10) and our two-band approximation [Eq. (11)], when the Fermi energy crosses the two middle bands $\epsilon_{2\mathbf{k}}^{(\pm)}$, it can be shown that the conventional part σ_{xy}^{s0} and the spin-torque-dipole part $\sigma_{xy}^{s\tau}$ of the conserved SHC are given by

$$\sigma_{xy}^{s0}=\frac{e}{4}\sum_{\mathbf{k}}\frac{f_{2\mathbf{k}}^{(-)}-f_{2\mathbf{k}}^{(+)}}{\Delta_{2\mathbf{k}}}\frac{\partial\epsilon_{2\mathbf{k}}^{(0)}}{\partial k_x}\frac{\partial\varphi_{2\mathbf{k}}}{\partial k_y} \tag{16}$$

and

$$\begin{aligned}\sigma_{xy}^{s\tau}&=\frac{e}{4}\sum_{\mathbf{k}}\frac{f_{2\mathbf{k}}^{(-)}-f_{2\mathbf{k}}^{(+)}}{\Delta_{2\mathbf{k}}}\left(\frac{\partial\varphi}{\partial k_x}\frac{\partial\epsilon_{2\mathbf{k}}^{(0)}}{\partial k_y}-2\frac{\partial\varphi_{2\mathbf{k}}}{\partial k_y}\frac{\partial\epsilon_{2\mathbf{k}}^{(0)}}{\partial k_x}\right)\\&\quad-\frac{e}{4}\sum_{\mathbf{k}}\left(\frac{\partial f_{2\mathbf{k}}^{(-)}}{\partial k_x}+\frac{\partial f_{2\mathbf{k}}^{(+)}}{\partial k_x}\right)\frac{\partial\varphi_{2\mathbf{k}}}{\partial k_y},\end{aligned} \tag{17}$$

where $f_{2\mathbf{k}}^{(\pm)}$ are the Fermi distribution functions for the middle bands $\epsilon_{2\mathbf{k}}^{(\pm)}$.

According to Kubo formulas (16) and (17), now let us see the first SHC plateau in Fig. 3 for $-2.0<\epsilon_F<0$. Since this plateau occurs upon occupation of the bottom (at the $\mathbf{\Gamma}$ point) of the middle bands, thus we can simplify the discussion of the first SHC plateau by expanding the middle-band Hamiltonian $\bar{H}_2(\mathbf{k})$ around the $\mathbf{\Gamma}$ point up to the first order in the Rashba coefficient λ,

$$\bar{H}_2^{\mathbf{\Gamma}}=-2.0+k^2+\lambda(k_y\sigma_x-k_x\sigma_y). \tag{18}$$

Not surprisingly, effective Rashba Hamiltonian (18) around the $\mathbf{\Gamma}$ point in the present kagome lattice is similar to that in the semiconductor 2DEG. Thus, as has been done in the 2DEG system,[42] a straightforward analytical calculation in terms of Eqs. (16)–(18) gives the zero-temperature SHC as $\sigma_{xy}^{s0}=-e/8\pi$, $\sigma_{xy}^{s\tau}=e/4\pi$, and subsequently $\sigma_{xy}^{s}=e/8\pi$. This analytical result is consistent with the numerical result in Fig. 3 for the first SHC plateau. Actually, the first SHC plateau in Fig. 3 goes beyond this analytical treatment around the $\mathbf{\Gamma}$ point and persists with increasing the Fermi energy up to $\epsilon_F=0$. The reason is attributed to the equivalent Fermi-surface topologies when changing ϵ_F within the interval $[-2.0,0]$. In fact, when ϵ_F lie in the region $[-2.0,0]$, the corresponding 2D Fermi surface consists of two simple closed loops circling around the $\mathbf{\Gamma}$ point, as illustrated in Fig. 2(b). Here, from Fig. 2(a) one can see that the critical value $\epsilon_F=0$ corresponds to the case that the Fermi surface nested in the middle bands touches the BZ edge at the $\mathbf{M}$ point, at which the energies of the two middle bands are degenerate due to the time-reversal symmetry.

When the Fermi level goes over this critical value, i.e., $\epsilon_F>0$, then the Fermi surface abruptly changes its topology.

Instead of simple closed loops, the Fermi surface for $0<\epsilon_F<1.0$ is characterized by six pieces of disconnected segments around six corners (**K** points) of the BZ as shown in Fig. 2(c). After gluing these segments together by a simple translation operation in the extended BZ, which does not change the property of electron states, then one can get two sets of closed loops around two **K** points as shown in Fig. 2(d). Thus the number of Fermi loops is doubled in the case of $0<\epsilon_F<1.0$ compared to the case of $-2.0<\epsilon_F<0$. This fundamental change in the Fermi-surface topology by increasing the electron filling, together with the combined fact that (i) the contributions from these two sets of **K**-centered Fermi loops are equivalent and (ii) the normal direction of the Fermi surface for $0<\epsilon_F<1.0$ is opposite to that for $-2.0<\epsilon_F<0$, results in a downward jump of SHC plateaus from $\sigma_{xy}^s=e/8\pi$ to $\sigma_{xy}^s=-e/4\pi$ at the critical value of $\epsilon_F=0$. To be more clear and to verify this argument based on the Fermi-surface topology, near each corner of the BZ let us expand the middle-band Hamiltonian $\bar{H}_2(\mathbf{k})$ up to the first order in the Rashba coefficient λ,

$$\bar{H}_2^{\mathbf{K}} = 1 - \sqrt{3}k - \lambda\frac{\sqrt{3}}{2k}(k_y\sigma_x - k_x\sigma_y), \tag{19}$$

where the wave vector **K** is coordinated with respect to the **K** point. By substitution of the eigenenergies and eigenstates of $\bar{H}_2^{\mathbf{K}}$ into Eqs. (16) and (17) and taking into account the six corners of the BZ, it is straightforward to obtain the zero-temperature SHC as $\sigma_{xy}^{s0}=e/4\pi$, $\sigma_{xy}^{s\tau}=-e/2\pi$, and $\sigma_{xy}^{s}=-e/4\pi$, which is consistent with the numerical result in Fig. 3.

Therefore, it becomes clear now that the different SHC plateaus in Fig. 3 are due to the different Fermi-surface topologies when varying ϵ_F. This observation makes it highly interesting to reinterpret the *metallic* SHE, similar to what has been done in discussing the metallic anomalous Hall effect (AHE),[45–48] in terms of Berry phases accumulated by adiabatic motion of electrons on the Fermi surface. The previous works have shown the relationship between the SHC and the Berry phase in the Rashba 2DEG.[6,49] The Fermi surface involved in those discussions is as simple as shown in Fig. 2(b). Compared to the Rashba 2DEG, one can see from the above discussions that the present kagome lattice provides more profound Fermi-surface topologies in the different regions of the electron filling. On one hand, in the regime $-2.0<\epsilon_F<0$ effective "Γ-valley" Hamiltonian (18) and the Fermi surface of the kagome lattice are identical to those of the Rashba 2DEG. As a result, the two kinds of systems have the same Berry-phase SHC in this regime. On the other hand, in the regime $0<\epsilon_F<1.0$ effective "**K**-valley" Hamiltonian (19) of the kagome lattice, which is absent in the Rashba 2DEG, has a remarkable Dirac-type spectrum with linear dependence of the energy on the electron momentum. Exploring the **K**-valley spintronics associated with Berry phases is the task of our following discussions.

The Berry phases of Bloch states $|u_{n\mathbf{k}}^{(\pm)}\rangle$ for closed paths $C_n^{(\pm)}$ in the k space are written as

$$\gamma_n^{(\pm)} = \oint_{\mathbf{C}_n^{(\pm)}} \mathbf{A}_{n\mathbf{k}}^{(\pm)}\cdot d\mathbf{k}, \tag{20}$$

where $\mathbf{C}_n^{(\pm)}$ are the Fermi loops identified by the zero-temperature Fermi distribution function $\Theta(\epsilon_F-\epsilon_{n\mathbf{k}}^{(\pm)})$ and

$$\mathbf{A}_{n\mathbf{k}}^{(\pm)} = \langle u_{n\mathbf{k}}^{(\pm)}|\left(-i\frac{\partial}{\partial\mathbf{k}}\right)|u_{n\mathbf{k}}^{(\pm)}\rangle \tag{21}$$

are the Berry connections. The corresponding Berry curvatures are defined as $\mathbf{\Omega}_{n\mathbf{k}}^{(\pm)}=\nabla_{\mathbf{k}}\times\mathbf{A}_{n\mathbf{k}}^{(\pm)}$. By substituting Eq. (21) into Eq. (9) and noting that $\sigma_{xy}^{s0}=-\sigma_{yx}^{s0}$, we have

$$\sigma_{xy}^{s0} = -\frac{e\hbar}{2}\sum_{\mu=+,-}\sum_{\mathbf{k}}\frac{f_{n\mathbf{k}}^{(\mu)}}{\epsilon_{n\mathbf{k}}^{(\mu)}-\epsilon_{n\mathbf{k}}^{(-\mu)}}[\mathbf{v}_{n\mathbf{k}}^{(0)}\times\mathbf{A}_{n\mathbf{k}}^{(\mu)}]_z, \tag{22}$$

where $\mathbf{v}_{n\mathbf{k}}^{(0)}=\frac{1}{\hbar}\frac{\partial\epsilon_{n\mathbf{k}}^{(0)}}{\partial\mathbf{k}}$ is the band velocity in the absence of the Rashba SO coupling. Now we focus our attention to the regime $0<\epsilon_F<1.0$, within which the gluing Fermi surface consists of two sets of loops around two **K** points as shown in Fig. 2(d). According to **K**-valley Hamiltonian (19) and its eigenenergies $\epsilon_{2\mathbf{k}}^{(\pm)}=1-\sqrt{3}k\pm\sqrt{3}\lambda/2$ and eigenstates $|u_{2\mathbf{k}}^{(\pm)}\rangle=\frac{1}{\sqrt{2}}(\mp ie^{-i\varphi_{2\mathbf{k}}},1)^{\mathrm{T}}$ with $\varphi_{2\mathbf{k}}=\tan^{-1}(k_y/k_x)$, it is straightforward to obtain the zero-temperature conventional SHC as

$$\sigma_{xy}^{s0} = 2\frac{e}{8\pi^2\lambda}\sum_{\mu=+,-}\mu\int_{\mathbf{S}_2^{(\mu)}} d^2\mathbf{k}\left[\frac{\mathbf{k}}{k}\times\mathbf{A}_{2\mathbf{k}}\right]_z, \tag{23}$$

where $\mathbf{S}_2^{(\mu)}$ $(\mu=+,-)$ in Eq. (23) denotes the integral area bounded by the Fermi loops $C_2^{(\mu)}$ [see Fig. 2(d)], and the Berry connections

$$\mathbf{A}_{2\mathbf{k}}^{(\pm)} = -\frac{1}{2}\frac{\partial\varphi_{2\mathbf{k}}}{\partial\mathbf{k}} = \frac{1}{2}\left(\frac{k_y}{k^2},-\frac{k_x}{k^2}\right) \equiv \mathbf{A}_{2\mathbf{k}} \tag{24}$$

are equivalent for the two middle bands. Note that the factor 2 in Eq. (23) is due to the contributions from the two **K** valleys. Clearly, if we define an Abelian spin gauge field $\mathcal{B}_{2\mathbf{k}}=(0,0,B)$, with $B=[\frac{\mathbf{k}}{k}\times\mathbf{A}_{2\mathbf{k}}]_z$, then Eq. (23) denotes a spin-flux difference through two areas $\mathbf{S}_2^{(+)}$ and $\mathbf{S}_2^{(-)}$. In virtue of this way, we define a spin gauge potential $\mathcal{A}_{2\mathbf{k}}$ to satisfy $\nabla_{\mathbf{k}}\times\mathcal{A}_{2\mathbf{k}}=\mathcal{B}_{2\mathbf{k}}$, then expression (23) for the conventional SHC is rewritten as

$$\begin{aligned}\sigma_{xy}^{s0} &= \frac{e}{4\pi^2\lambda}\sum_{\mu=+,-}\mu\int_{\mathbf{S}_2^{(\mu)}}\mathcal{B}_{2\mathbf{k}}\cdot d\mathbf{S}\\ &= \frac{e}{4\pi^2\lambda}\sum_{\mu=+,-}\mu\int_{\mathbf{S}_2^{(\mu)}}\nabla_{\mathbf{k}}\times\mathcal{A}_{2\mathbf{k}}\cdot d\mathbf{S}\\ &= \frac{e}{4\pi^2\lambda}\sum_{\mu=+,-}\mu\oint_{\mathbf{C}_2^{(\mu)}}\mathcal{A}_{2\mathbf{k}}\cdot d\mathbf{k}.\end{aligned} \tag{25}$$

We choose a symmetric form for the spin gauge potential $\mathcal{A}_{2\mathbf{k}}$,

$$\mathcal{A}_{2\mathbf{k}} = \frac{1}{2}\left(\frac{k_y}{k},-\frac{k_x}{k}\right) = k\mathbf{A}_{2\mathbf{k}}, \tag{26}$$

which obviously satisfies $\nabla_{\mathbf{k}}\times\mathcal{A}_{2\mathbf{k}}=\mathcal{B}_{2\mathbf{k}}$. By substitution of Eq. (26) into Eq. (25), we have

$$\sigma_{xy}^{s0} = \frac{e}{4\pi^2\lambda} \sum_{\mu=+,-} \mu \oint_{\mathbf{C}_2^{(\mu)}} k\mathbf{A}_{2\mathbf{k}} \cdot d\mathbf{k} = \frac{e}{4\pi^2} \sum_{\mu=+,-} \frac{\mu k_F^{(\mu)}}{k_F^{(+)} - k_F^{(-)}} \gamma_2^{(\mu)}, \tag{27}$$

where $k_F^{(\pm)}$ are the Fermi wave vectors for the two middle bands $\epsilon_{2\mathbf{k}}^{(\pm)} = 1 - \sqrt{3}k \pm \sqrt{3}\lambda/2$, and we have used the fact that $k_F^+ - k_F^- = \lambda$. Thus, we get a remarkable relationship between the conventional SHC and Berry phases for the **K**-valley Hamiltonian. Using the chosen middle-band eigenstates given above Eq. (23), it is simple to obtain the Berry phases as $\gamma_2^{(+)} = \gamma_2^{(-)} = \pi$, leading Eq. (27) to $\sigma_{xy}^{s0} = \frac{e}{4\pi}$, consistent again with the numerical result in Fig. 3(b).

In summary, we have theoretically investigated the metallic spin Hall effect in the 2D kagome lattice with Rashba SO coupling. When varying the Fermi energy ϵ_F, we have found that the conserved SHC σ_{xy}^s and its two components, i.e., the conventional term σ_{xy}^{s0} and the spin-torque-dipole term $\sigma_{xy}^{s\tau}$, are characterized by a series of plateaus, which is absent in the simple 2DEG system. In the whole range ϵ_F varies, the two terms σ_{xy}^{s0} and $\sigma_{\mu\nu}^{s\tau}$ have opposite contributions. The magnitude of $\sigma_{\mu\nu}^{s\tau}$ is twice that of $\sigma_{\mu\nu}^{s0}$. It has been shown that these SHC plateaus in the different regions of ϵ_F are closely associated with the topologically different Fermi surfaces surrounding the high-symmetry BZ points, i.e., the **Γ** and **K** points. Thus, as has been revealed in this paper, a relationship between these SHC plateaus and Berry phases accumulated by adiabatic motion of quasiparticles on the Fermi surfaces can be built up, which is similar to the metallic AHE. In particular, we have shown that compared to the case with the Fermi surface encircling the **Γ** point, the amplitude of the SHC with the Fermi surface encircling the **K** points is twice as large. Considering the combined fact that (i) the 2D kagome lattice is the line graph of the honeycomb structure, (ii) the Rashba SO coupling and the Fermi surface surrounding the **K** points can be easily realized in the graphene with honeycomb structure, and (iii) the similar Berry-phase AHE has been recently observed, we expect that the present prediction of the **K** valley enhanced SHE can be observed in the graphene system.

P.Z. was supported by the NSFC under Grants No. 10604010 and No. 10534030, and by the National Basic Research Program of China (973 Program) under Grant No. 2009CB929103. S.-S.L. was supported by the NSFC under Grants No. 60776061 and No. 60521001.

*Corresponding author. zhang_ping@iapcm.ac.cn

[1] G. A. Prinz, Science **282**, 1660 (1998); S. A. Wolf, D. D. Awschalom, R. A. Buhrman, J. M. Daughton, S. von Molnár, M. L. Roukes, A. Y. Chtchelkanova, and D. M. Treger, *ibid.* **294**, 1488 (2001).
[2] *Semiconductor Spintronics and Quantum Computation*, edited by D. D. Awschalom, N. Sarmarth, and D. Loss (Springer-Verlag, Berlin, 2002).
[3] I. Zutic, J. Fabian, and S. D. Sarma, Rev. Mod. Phys. **76**, 323 (2004).
[4] S. Murakami, N. Nagaosa, and S. C. Zhang, Science **301**, 1348 (2003); Phys. Rev. B **69**, 235206 (2004).
[5] J. Sinova, D. Culcer, Q. Niu, N. A. Sinitsyn, T. Jungwirth, and A. H. MacDonald, Phys. Rev. Lett. **92**, 126603 (2004).
[6] S.-Q. Shen, Phys. Rev. B **70**, 081311(R) (2004).
[7] D. Culcer, J. Sinova, N. A. Sinitsyn, T. Jungwirth, A. H. MacDonald, and Q. Niu, Phys. Rev. Lett. **93**, 046602 (2004).
[8] J. I. Inoue, G. E. W. Bauer, and L. W. Molenkamp, Phys. Rev. B **70**, 041303(R) (2004).
[9] E. I. Rashba, Phys. Rev. B **70**, 161201(R) (2004).
[10] B. A. Bernevig, J. P. Hu, E. Mukamel, and S.-C. Zhang, Phys. Rev. B **70**, 113301 (2004).
[11] J. Schliemann and D. Loss, Phys. Rev. B **71**, 085308 (2005).
[12] G. Y. Guo, Y. Yao, and Q. Niu, Phys. Rev. Lett. **94**, 226601 (2005).
[13] B. A. Bernevig and S.-C. Zhang, Phys. Rev. Lett. **95**, 016801 (2005).
[14] B. K. Nikolić, S. Souma, L. P. Zârbo, and J. Sinova, Phys. Rev. Lett. **95**, 046601 (2005).
[15] Q.-F. Sun and X. C. Xie, Phys. Rev. B **72**, 245305 (2005).
[16] Y. K. Kato, R. C. Myers, A. C. Gossard, and D. D. Awschalom, Science **306**, 1910 (2004).
[17] J. Wunderlich, B. Kaestner, J. Sinova, and T. Jungwirth, Phys. Rev. Lett. **94**, 047204 (2005).
[18] V. Sih, R. C. Myers, Y. K. Kato, W. H. Lau, A. C. Gossard, and D. D. Awschalom, Nat. Phys. **1**, 31 (2005).
[19] V. Sih, W. H. Lau, R. C. Myers, V. R. Horowitz, A. C. Gossard, and D. D. Awschalom, Phys. Rev. Lett. **97**, 096605 (2006).
[20] S. Murakami, N. Nagaosa, and S.-C. Zhang, Phys. Rev. Lett. **93**, 156804 (2004).
[21] C. L. Kane and E. J. Mele, Phys. Rev. Lett. **95**, 226801 (2005).
[22] C. L. Kane and E. J. Mele, Phys. Rev. Lett. **95**, 146802 (2005).
[23] M. Onoda and N. Nagaosa, Phys. Rev. Lett. **95**, 106601 (2005).
[24] B. A. Bernevig and S.-C. Zhang, Phys. Rev. Lett. **96**, 106802 (2006).
[25] X.-L. Qi, Y.-S. Wu, and S.-C. Zhang, Phys. Rev. B **74**, 085308 (2006).
[26] D. N. Sheng, Z. Y. Weng, L. Sheng, and F. D. M. Haldane, Phys. Rev. Lett. **97**, 036808 (2006).
[27] T. Fukui and Y. Hatsugai, Phys. Rev. B **75**, 121403(R) (2007).
[28] L. Fu and C. L. Kane, Phys. Rev. B **74**, 195312 (2006).
[29] L. Fu, C. L. Kane, and E. J. Mele, Phys. Rev. Lett. **98**, 106803 (2007).
[30] L. Fu and C. L. Kane, Phys. Rev. B **76**, 045302 (2007).
[31] M. Onoda, Y. Avishai, and N. Nagaosa, Phys. Rev. Lett. **98**, 076802 (2007).
[32] C. Wu, B. A. Bernevig, and S.-C. Zhang, Phys. Rev. Lett. **96**, 106401 (2006).
[33] C. Xu and J. E. Moore, Phys. Rev. B **73**, 045322 (2006).
[34] B. A. Bernevig, T. L. Hughes, and S.-C. Zhang, Science **314**, 1757 (2006).
[35] J. E. Moore and L. Balents, Phys. Rev. B **75**, 121306(R) (2007).
[36] P. Mohan, F. Nakajima, M. Akabori, J. Motohisa, and T. Fukui, Appl. Phys. Lett. **83**, 689 (2003); P. Mohan, J. Motohisa, and T.

Fukui, *ibid.* **84**, 2664 (2004).
[37] M. J. Higgins, Y. Xiao, S. Bhattacharya, P. M. Chaikin, S. Sethuraman, R. Bojko, and D. Spencer, Phys. Rev. B **61**, R894 (2000); Y. Xiao, D. A. Huse, P. M. Chaikin, M. J. Higgins, S. Bhattacharya, and D. Spencer, *ibid.* **65**, 214503 (2002).
[38] S. Y. Tong, G. Xu, W. Y. Hu, and M. W. Puga, J. Vac. Sci. Technol. B **3**, 1076 (1985).
[39] K. Shiraishi, H. Tamura, and H. Takayanagi, Appl. Phys. Lett. **78**, 3702 (2001).
[40] J. Shi, P. Zhang, D. Xiao, and Q. Niu, Phys. Rev. Lett. **96**, 076604 (2006).
[41] P. Zhang and Q. Niu, arXiv:cond-mat/0406436 (unpublished).
[42] P. Zhang, Z. Wang, J. Shi, D. Xiao, and Q. Niu, Phys. Rev. B **77**, 075304 (2008).
[43] A. Mielke, J. Phys. A **24**, L73 (1991); **24**, 3311 (1991); **25**, 4335 (1992).
[44] To simply clarify this feature, let us consider a usual Anderson insulator, in which the eigenenergy states are localized and thus the spin displacement operator $s_z\mathbf{r}$ is well defined. Since the conserved spin current $\mathcal{J}_s$ is given as a time derivative of the spin displacement operator, then it is straightforward to see that the response coefficient σ_{xy}^s of $\mathcal{J}_s$ to a weak electric field is zero although both of the two components σ_{xy}^{s0} and $\sigma_{xy}^{s\tau}$ in σ_{xy}^s can be nonzero. This subsequently results in the conclusion that these two components have different signs.
[45] T. Jungwirth, Q. Niu, and A. H. MacDonald, Phys. Rev. Lett. **88**, 207208 (2002).
[46] Z. Fang, N. Nagaosa, K. S. Takahashi, A. Asamitsu, R. Mathieu, T. Ogasawara, H. Yamada, M. Kawasaki, Y. Tokura, and K. Terakura, Science **302**, 92 (2003).
[47] Y. Yao, L. Kleinman, A. H. MacDonald, J. Sinova, T. Jungwirth, D.-S. Wang, E. Wang, and Q. Niu, Phys. Rev. Lett. **92**, 037204 (2004).
[48] F. D. M. Haldane, Phys. Rev. Lett. **93**, 206602 (2004).
[49] T.-W. Chen, C.-M. Huang, and G. Y. Guo, Phys. Rev. B **73**, 235309 (2006).